Appl. Phys. A (2017) 123:380
DOI 10.1007/s00339-017-1002-6

Applied Physics A
Materials Science & Processing

Optimization and realization of symmetric multilayer cascaded FSSs structure with excellent Butterworth response at large angle incidence

Yang Xu[1,2] · Jinsong Gao[1,2] · Nianxi Xu[1] · Hai Liu[1] · Dongzhi Shan[1] · Naitao Song[1]

Received: 11 March 2017 / Accepted: 25 April 2017 / Published online: 27 April 2017

Abstract A simple and fast optimization method for symmetric multilayer frequency selective surfaces (FSSs) structure is presented in this paper, based on the mutual admittance approach. To elaborate the proposed method, a symmetric bi-planar FSSs structure is selected to explain the optimizing process. After the optimized analysis, the symmetric bi-planar FSSs structure can achieve good characteristics of flat top and sharp roll-off at 70° angle of incidence, with an optimum coupling layer medium ($d_2 = 15$ mm, $\varepsilon_2 = 1.15$). As it is difficult to obtain the material with $\varepsilon = 1.15$ by using traditional technique, we design an array of dielectric cylinders to effectively replace the homogeneous medium, based on the theory of periodic waveguide. To verify the optimization method and design idea, a prototype simple of the symmetric bi-planar FSS is fabricated and measured. The measured results of the prototype well coincided with the simulation results, which further shows the validity of the optimization method and the idea of equivalent substitution.

✉ Jinsong Gao
gaojs999@163.com

[1] Key Laboratory of Optical System Advanced Manufacturing Technology, Changchun Institute of Optics, Fine Mechanics and Physics, Chinese Academy of Sciences, Changchun 130033, China

[2] University of the Chinese Academy of Sciences, Beijing 100039, China

1 Introduction

As an artificial electromagnetic periodic structure, frequency selective surface (FSS) consists of two dimensional arrays of metallic patches or apertures on dielectric layers, performing special filtering effect, such as band-pass and band-stop responses. Commonly, the band-pass FSSs are applied in the design of radomes, satellites and aircrafts for the use of radar cross section (RCS) reduction [1–3]. Besides that, they also own enormous potentials in the telecommunication domains, for instance, design of antenna [4, 5]. Whatever the band-pass FSS is used for, an ideal filtering response with flat top, fast roll-off and high transmittance is always demanded.

In practical applications, to achieve broadband band-pass FSS, a very simple method is proposed via cascading multiple identical surfaces behind each other. As illustrated in Ref. [6], a symmetric bi-planar FSSs structure can generate flat top and sharp roll-off response (Butterworth response) at crucial coupling under minor incident angles. With the increase of incident angle, the Butterworth response is destroyed and a valley appears in the center frequency, resulting in a decline of the transmittance. In general, to design an ideal Butterworth response at large angle incidence, such as 70°, verifying the optimum coupling, namely the thickness and permittivity of the intermediate layer medium, becomes very important. To achieve the ideal match, repeatedly iterative computation analyses are operated by utilizing genetic algorithm [7, 8] or Taguchi's method [9], which would inevitably consume massive time and resources. Although there are several methods have been proposed recently to deal with the problem of optimum coupling [10–12], they possess several defects more or less, such as only considering the optimum coupling at normal incidence [10, 11] or the

simulation of single FSS is still demanded [12]. Furthermore, even if the optimization results are figured out after a large amount of work, sometimes we are confronted with the issue that the optimum permittivity does not exist in natural material and cannot be obtained by using traditional techniques.

In this paper, a simple and fast optimizing method based on the analysis of self-admittance and mutual admittance is presented for symmetric N layers FSSs structure. To account for the process of optimization in detail, a symmetric bi-planar FSSs structure is chosen as an example. For the exemplary structure with specified structural parameters, through contrasting the ratio $|Y^{2,1}|/Y_{0\mathrm{re}}$ for TE and TM polarizations from 0° to 80°, the optimum parameters of $d_2 = 15$ mm and $\varepsilon_2 = 1.15$ for the intermediate layer medium can be confirmed fast and efficiently. As it is difficult to obtain the material with permittivity of 1.15 using traditional techniques, an array of dielectric cylinders made of Teflon is designed based on the theory of periodic waveguides, to equivalently substitute the homogeneous intermediate layer medium. To verify the correctness of the optimizing method and ensure that the equivalent substitution is reasonable, a prototype is fabricated and tested for TE polarization from 0° to 70°. The test results show that the prototype still maintains an excellent filtering property with a flat top of about 400 MHz and a high transmission of more than 80% at the incident angle of 70°.

2 Optimizing method and analysis

From an electrical design point of view, for N layers identical FSS cascaded structure with $N + 1$ layers medium, the symmetric design in general is far superior to the nonsymmetric design. Therefore, here we concentrate on the symmetric case. Based on the mutual admittance approach, the transmission coefficient of symmetric N layers lossless FSS structure (T_N) can be determined by the following equations [13]:

$$T_N = \frac{1}{\sqrt{1+P_N^2}} = \frac{2Y_{0\mathrm{re}}^{1,1}\left|Y^{2,1}\right|\left|Y^{3,2}\right|\cdots\left|Y^{N,N-1}\right|}{|D_N|} \tag{1}$$

$$D_N = \begin{bmatrix} Y^{1,1} & Y^{1,2} & 0 & 0 & \cdots & 0 \\ Y^{2,1} & Y^{2,2} & Y^{2,3} & 0 & \cdots & 0 \\ 0 & Y^{3,2} & Y^{3,3} & Y^{3,4} & \cdots & 0 \\ \vdots & \vdots & \vdots & \vdots & \vdots & \vdots \\ 0 & \cdots & 0 & 0 & Y^{N,N-1} & Y^{N,N} \end{bmatrix} \tag{2}$$

where $Y^{n,n}$ ($n = 1,2,\ldots,N$) is the self-admittance of the nth layer FSS, $Y^{m,n}$ ($m \neq n$) is the mutual admittance between the mth and nth layer FSSs, $|D_N|$ is the determinant of square matrix D_N denoted by Eq. (2), and P_N is a polynomial of order N as a function of $Y^{n,n}$ and $Y^{m,n}$. As all N layers of FSS are identical and the structure is symmetric, the self-admittance and mutual admittance in above equations satisfy the relations as follows:

$$Y^{1,1} = Y^{2,2} = \cdots = Y^{N,N} = Y_{0\mathrm{re}} + jY_{0\mathrm{im}} \tag{3}$$

$$Y^{1,2}(=Y^{2,1}) = Y^{2,3}(=Y^{3,2}) = \cdots = Y^{N-1,N}(=Y^{N,N-1}) \tag{4}$$

where $Y_{0\mathrm{re}}$ and $Y_{0\mathrm{im}}$ denote the real part and imaginary part of the self-admittance, respectively, for each FSS. Through using Eqs. (1)–(4), the relationship of T_N (P_N) with respect to $Y^{1,1}$ and $Y^{2,1}$, namely $T_N(Y^{1,1},Y^{2,1})$ or $P_N(Y^{1,1},Y^{2,1})$, can be established for symmetric N layers lossless FSS structure.

In general, the imaginary part of the self-admittance ($Y_{0\mathrm{im}}$) is more sensitive to the frequency variations than its real part ($Y_{0\mathrm{re}}$) and the mutual-admittance ($Y^{2,1}$) [14]. Therefore, the extremes of transmission coefficient (T_N) can be obtained by differentiation with respect to $Y_{0\mathrm{im}}$, which yields $P_N(\mathrm{d}P_N/\mathrm{d}Y_{0\mathrm{im}}) = 0$ with roots $P_N = 0$ and $\mathrm{d}P_N/\mathrm{d}Y_{0\mathrm{im}} = 0$. The former root corresponds to the maxima with unit transmission, while the latter represents the minima, meaning the destruction of flat top and appearance of the valley. Obviously, when the two roots are validated at the same frequency, the valley would disappear and an ideal Butterworth response is obtained. Thereby, by analyzing the two roots, the relation between $Y^{1,1}$ and $Y^{2,1}$ is determined finally, that is, the Butterworth response can be achieved through properly setting the relation of $Y^{1,1}$ and $Y^{2,1}$ for symmetric N layers FSS structure. To further explain the aforementioned analysis method in detail, here the optimizing process of a symmetric bi-planar FSSs structure is shown as follows.

As shown in Fig. 1a, the investigated traditional symmetric bi-planar FSSs consist of two identical FSSs sandwiched between three layer medium slabs. The permittivity and thickness of the top layer medium slab is the same as that of the bottom one, which are ε_1 and d_1, respectively. The intermediate medium layer with permittivity of ε_2 and thickness of d_2 acts as the coupling layer. Figure 1b shows the top view of the unit cell of the proposed FSS. To achieve good stability to angle of incidence [15], the circular loop slot pattern is chosen here as the unit cell. Each unit cell has the physical dimensions of D_x and D_y in the x and y directions. The inner and outer radii of the circular loop are represented by r and R, respectively.

Based on the mutual admittance approach mentioned above, the transmission curve of the symmetric bi-planar FSSs is related to the mutual admittance between array 1 and array 2 ($Y^{2,1}$) together with the self-admittance of array 1 or array 2 ($Y_{0\mathrm{re}} + \mathrm{j}Y_{0\mathrm{im}}$). From Eqs. (1) and (2), P_2 is calculated as follows:

$$P_2 = \frac{1}{2}\frac{Y_{0\mathrm{re}}}{|Y^{2,1}|}\left[\left(\frac{Y_{0\mathrm{im}}}{Y_{0\mathrm{re}}}\right)^2 - \left(\frac{|Y^{2,1}|^2}{Y_{0\mathrm{re}}^2} - 1\right)\right] \tag{5}$$

By analysis of the roots $P_2 = 0$ and $\mathrm{d}P_2/\mathrm{d}Y_{0\mathrm{im}} = 0$, we can obtain that the maxima and minima are located at $Y_{0\mathrm{im}}^{\max} = \pm Y_{0\mathrm{re}}\sqrt{(|Y^{2,1}|/Y_{0\mathrm{re}})^2 - 1}$ and $Y_{0\mathrm{im}}^{\min} = 0$, respectively. When the ratio of $|Y^{2,1}|/Y_{0\mathrm{re}}$ equals to one, namely $Y_{0\mathrm{im}}^{\max} = Y_{0\mathrm{im}}^{\min}$, a maximally flat top and sharp roll-off transmission response (Butterworth response) can be obtained. For the case of $|Y^{2,1}|/Y_{0\mathrm{re}} > 1$, the characteristic of flat top is destroyed and a valley appears in the middle of top, which cause the decline of transmission. While, as the value of $|Y^{2,1}|/Y_{0\mathrm{re}}$ becomes much less than one, such as 0.6, an unsatisfactory curve with low transmission (<80%), narrow flat top and slow roll-off is obtained. To realize the ideal Butterworth response for symmetric bi-planar FSSs structure, the typical value of $|Y^{2,1}|/Y_{0\mathrm{re}}$ would be between 0.98 and 1.1 [16].

From Ref. [16], the mutual admittance $Y^{2,1}$ and the real part of self-admittance $Y_{0\mathrm{re}}$ are obtained as follows:

$$Y^{2,1} = \frac{Y_2}{2D_xD_y}\sum_m\sum_n \frac{1}{r_{2z}}\left[{}_{\perp}P_2^{(1)}\,{}_{\perp}P_2^{(2)t} + {}_{\parallel}P_2^{(1)}\,{}_{\parallel}P_2^{(2)t}\right]\frac{2j}{\sin(\beta_2 d_2 r_{2z})} \tag{6}$$

$$Y_{0\mathrm{re}} = \frac{Y_1}{2D_xD_y}\frac{1}{r_{1z}}\left[{}_{\perp}P_1^{(1)}\,{}_{\perp}P_1^{(1')t}\mathrm{Re}_{\perp}T + {}_{\parallel}P_1^{(1)}\,{}_{\parallel}P_1^{(1')t}\mathrm{Re}_{\parallel}T\right] \tag{7}$$

where $Y_1 = \sqrt{\varepsilon_1}$ and $Y_2 = \sqrt{\varepsilon_2}$ are the intrinsic admittance of top layer and intermediate layer medium, respectively, $r_{1z} = \cos\theta_1$ is the cosine functions of refractive angle in top layer medium and

$$r_{2z} = \begin{cases} \cos\theta_2 & \text{for } m,n = 0 \\ -j\sqrt{\left(\sin\theta_2\cos\phi + m\frac{2\pi}{D_x}\right)^2 + \left(\sin\theta_2\sin\phi + n\frac{2\pi}{D_x}\right)^2 - 1} & \text{for } m,n \neq 0 \end{cases}$$

is the normalized wave vector of z component in intermediate layer medium, $\beta_2 = 2\pi/\lambda_2$ is the propagation constant in intermediate layer medium, ${}_{\perp}P_1^{(1)}$, ${}_{\perp}P_1^{(1')t}$, ${}_{\parallel}P_1^{(1)}$, ${}_{\parallel}P_1^{(1')t}$ and ${}_{\perp}P_2^{(1)}$, ${}_{\perp}P_2^{(2)t}$, ${}_{\parallel}P_2^{(1)}$, ${}_{\parallel}P_2^{(2)t}$ are, respectively, pattern functions of array 1 and array 2 for both vertical and horizontal polarizations, and ${}_{\perp}T$ as well as ${}_{\parallel}T$ are transformation functions under vertical and horizontal polarizations. As the pattern functions represent the distributions of surface current in FSS [16], these pattern functions for symmetric bi-planar FSSs structure satisfy the following equations:

$$\begin{aligned} {}_{\perp}P_1^{(1)} = {}_{\perp}P_1^{(1')t} = {}_{\perp}P_2^{(1)} = {}_{\perp}P_2^{(2)t} = {}_{\parallel}P_1^{(1)} = {}_{\parallel}P_1^{(1')t} \\ = {}_{\parallel}P_2^{(1)} = {}_{\parallel}P_2^{(2)t} \end{aligned} \tag{8}$$

From Eq. (8), we get that the values of $|Y^{2,1}|/Y_{0\mathrm{re}}$ for both polarizations are independent with these pattern functions, which would simplify the calculation of $|Y^{2,1}|/Y_{0\mathrm{re}}$. As for transformation functions, they do not have physical significance and just are used for mathematical computation. The real part of the transformation functions are defined as follows [16]:

$$\mathrm{Re}_{\perp}T = \frac{(Y_0/r_{0z})^2\cdot(1-\cos 2\beta_1 d_1 r_{1z}) + (Y_1/r_{1z})^2\cdot(1+\cos 2\beta_1 d_1 r_{1z})}{2\cdot(Y_0/r_{oz})\cdot(Y_1/r_{1z})} \tag{9}$$

$$\mathrm{Re}_{\parallel}T = \frac{(Y_0 r_{0z})^2\cdot(1-\cos 2\beta_1 d_1 r_{1z}) + (Y_1 r_{1z})^2\cdot(1+\cos 2\beta_1 d_1 r_{1z})}{2\cdot(Y_0 r_{oz})\cdot(Y_1 r_{1z})} \tag{10}$$

where Y_0 is the intrinsic admittance of vacuum, $r_{0z} = \cos\theta_0$ is the cosine of incident angle, and $\beta_1 = 2\pi/\lambda_1$ is the propagation constant in top or bottom layer medium. Note here that, contrary to the usual definition, the vertical and horizontal polarizations correspond to the TM and TE polarizations, respectively.

According to the Eq. (6), the mutual admittance $Y^{2,1}$ is described by the sum of a series of different order modes. When there is no grating lobes at the working band, the principal mode ($m = n = 0$) represent the part of $Y^{2,1}$ introduced by propagating waves, while the other high order modes ($m, n \neq 0$) are contributed by the evanescent waves. As the evanescent waves cannot propagate to far field region, the mutual admittance can be calculated by just considering the principal mode when the electrical thickness of intermediate medium is large enough. In general, the high order mode terms can be ignored when the ratio between the lowest order evanescent modes (m, $n = \pm 1, 0$) and the propagating mode ($m = n = 0$) is less than 0.01, namely Modes(±1,0)/Mode(0,0) <0.01. By using the Eq. (6), the ratio Modes(±1,0)/Mode(0,0) is acquired, which suffices the following relation:

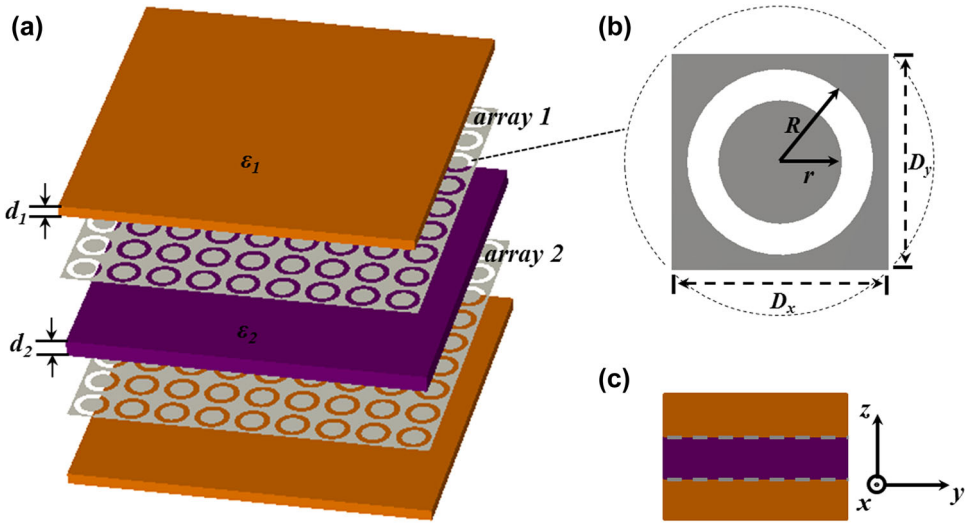

Fig. 1 Topology of the symmetric bi-planar FSS structure. **a** Three-dimensional view, **b** top view of the unit cell and **c** side view

$$\frac{\text{Modes}(\pm 1,0)}{\text{Mode}(0,0)} = 4\frac{\sin\left(\frac{2\pi}{\lambda_0}\sqrt{\varepsilon_2}d_2\right)}{\sqrt{\frac{1}{\varepsilon_2}\left(\frac{\lambda_0}{D_x}\right)^2 - 1}} e^{-\frac{2\pi}{\lambda_0}d_2\sqrt{\left(\frac{\lambda_0}{D_x}\right)^2-\varepsilon_2}} \tag{11}$$

Calculated using the Eqs. (6)–(10), the distribution of $|Y^{2,1}|/Y_{0\text{re}}$ with respect to d_2 and ε_2 is shown in Fig. 2a at working frequency 7 GHz under normal incidence. Based on the aforementioned analysis, the thickness of intermediate medium d_2 and corresponding permittivity ε_2 should satisfy the inequality $0.98 < |Y^{2,1}|/Y_{0\text{re}} < 1.1$, as depicted by the Line 1 and the Line 2 in Fig. 2a. Here, a widely used coating material with $\varepsilon_1 = 3.17$ and $d_1 = 3$ mm is selected as the top and bottom layer slabs. The dimensions of unit cell are $D_x = D_y = 14$ mm, $r = 4$ mm and $R = 6$ mm. These two lines indicate that there are two values of d_2 excited for each value of ε_2, which can be attributed to the sine function item contained in the Eq. (6). In addition, the Line 2 represents a larger electrical thickness than Line 1. Figure 2b shows the values of Modes(±1,0)/Mode(0,0) with respect to the d_2 and ε_2 under normal incidence at 7 GHz, which is obtained by using the Eq. (9). It is observed from the right part of the Fig. 2b that, the ratio between Modes(±1,0) and Mode(0,0) will increase with the increment of ε_2 and the diminishment of d_2. While in the shaded region (left part) of Fig. 2b, where the ratio Modes(±1,0)/Mode(0,0) is less than 0.01, the influence of the evanescent waves can be negligible compared with the propagating waves. Hence, by combining the Fig. 2a with the Fig. 2b, the range of the optimizing thickness d_2 and corresponding permittivity ε_2 can be verified, as shown in the Fig. 3.

By applying the optimized d_2 and ε_2 to the Eqs. (6)–(10), the ratio of $|Y^{2,1}|$ to $Y_{0\text{re}}$ with respect to optimizing ε_2 for TE and TM polarizations from 0° to 80° can be obtained and plotted in Fig. 4. As shown in Fig. 4, for each value of ε_2, the ratio $|Y^{2,1}|/Y_{0\text{re}}$ shows a trend from decline to rise when the incident angle is increased from 0° to 80° for both TE and TM polarizations. For TE polarization, the value of $|Y^{2,1}|/Y_{0\text{re}}$ at oblique incidence is improved with the increment of ε_2, as shown in Fig. 4a. Conversely, for TM polarization at larger incident angle, such as 60°, 70°, 80°, as depicted in Fig. 4b, the ratio $|Y^{2,1}|/Y_{0\text{re}}$ decline with the growth of ε_2. It's obvious that the ratio $|Y^{2,1}|/Y_{0\text{re}}$ is always larger than 1.1 at the incident angle of 80° for both TE and TM polarizations, whatever ε_2 is. This means that a valley will inevitably appear at 80° incidence. To ensure the Butterworth response at various incident angles from 0° to 70° as much as possible for both TE and TM polarizations, the value of $|Y^{2,1}|/Y_{0\text{re}}$ should be always close to one, and thereby we choose 1.15 as the optimizing ε_2 and the corresponding thickness d_2 is 15 mm. The transmission curves of the optimizing structure at various incident angles are obtained by using full-wave simulation software CST for TE and TM polarizations, as shown in Fig. 5. Floquet ports and unit -cell boundaries are applied to mimic the infinite structure. These curves certainly retain the good characteristics of broad flat top and sharp roll-off at larger incident angle, except the evident frequency shift for TM polarization, which is caused by the admittance mismatch of top or bottom layer medium. The insertion loss is caused by the tangent loss of top and bottom layer medium, which is set as 0.008 in the full-wave simulation.

3 Design of optimizing medium

As it is very difficult and expensive to fabricate the intermediate layer medium with aforementioned optimizing permittivity 1.15 using traditional techniques, here we design an array of dielectric cylinder to substitute the

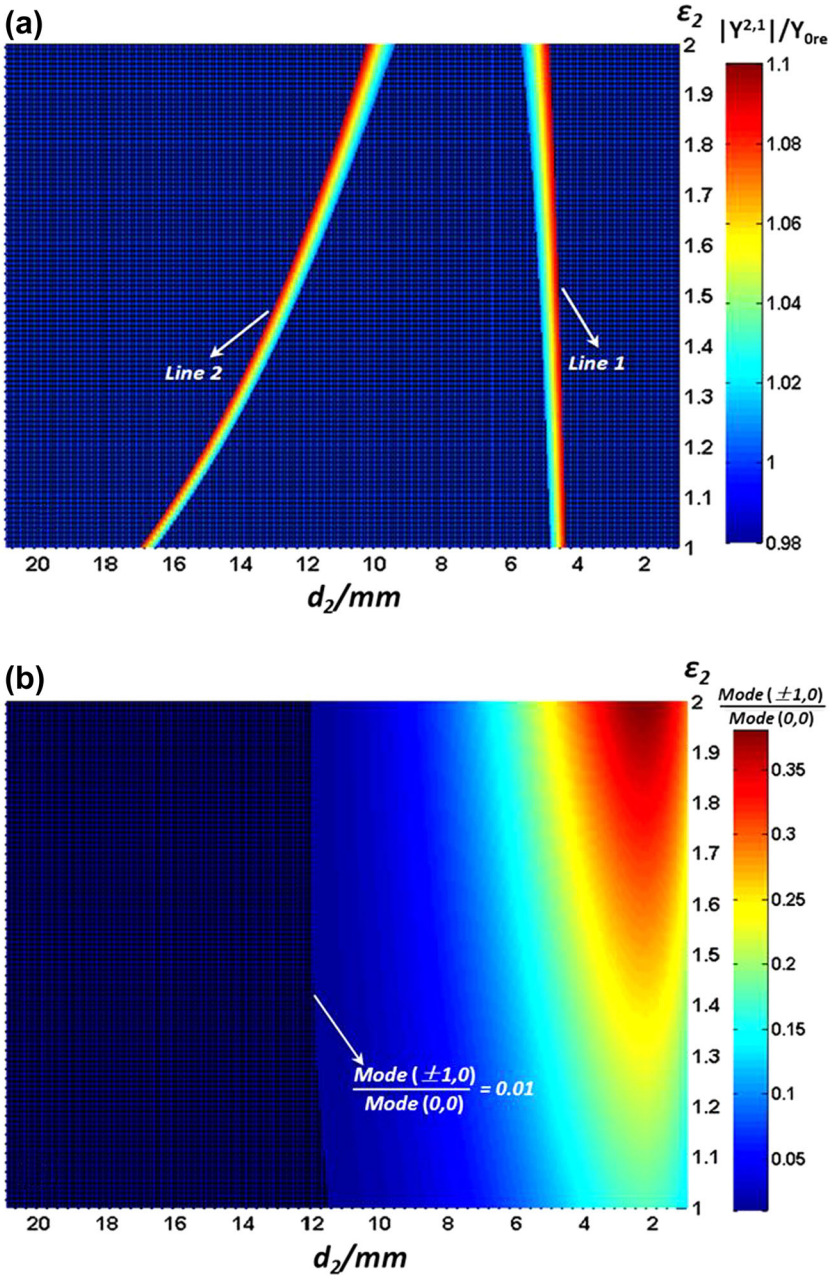

Fig. 2 **a** The distribution of $|Y^{2,1}|/Y_{0re}$ with respect to ε_2 and d_2 under normal incidence at 7 GHz, and **b** the corresponding distribution of Modes(±1,0)/Mode(0,0) with respect to the d_2 and ε_2

intermediate layer medium, based on the theory of periodic waveguides [17]. The new-type symmetric bi-planar FSSs structure is shown in Fig. 6. The radius and period of the dielectric cylinders are identical to the inner radius and period of the circular loop slots, and the dielectric cylinder and circular loop slot are totally coaxial. The array of dielectric cylinder can be considered as a birefringent homogenous material due to the fact that the size of the cylinders ($r = 4$ mm) is smaller compared with the working wavelength (about 43 mm). By retaining only the zeroth order terms in the eigenvalue equations for the vertical and horizontal polarizations, the approximate effective permittivity can be derived from the theory of periodic waveguides. This procedure gives the following equations [18]:

$$\varepsilon_{\perp}^{eff} = \left[f\varepsilon_d^{-1} + (1-f)\varepsilon_a^{-1}\right]^{-1} \tag{12}$$

for the vertical polarization and

$$\varepsilon_{\parallel}^{eff} = [f\varepsilon_d + (1-f)\varepsilon_a] \tag{13}$$

for the horizontal polarization. Permittivity of the dielectric cylinder and air are denoted by ε_d and ε_a, and $f = \pi\left(\frac{r}{D_x}\right)^2$ stands for the fill factor of dielectric cylinder.

To achieve the optimizing permittivity 1.15, the material of dielectric cylinder we choose is Teflon with permittivity

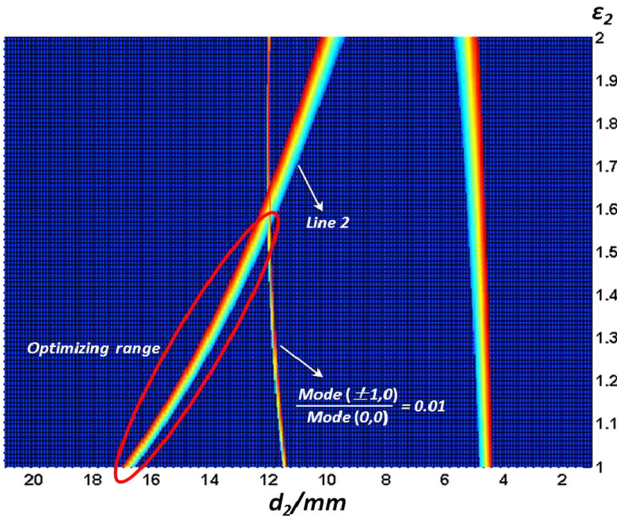

Fig. 3 The optimizing range of ε_2 and d_2 verified by combing Fig. 2a, b, where the Butterworth response at normal incidence can be obtained

of 2.1 and tangent loss of 0.0002, and the fill factor should be about 0.25 with $r = 4$ mm and $D_x = 14$ mm. By applying these parameters to Eqs. (12) and (13), the approximate effective permittivity for the vertical and horizontal polarizations can be obtained and the results are as follows: $\varepsilon_{\perp}^{eff} \approx 1.15$ and $\varepsilon_{\parallel}^{eff} \approx 1.28$. As shown in Fig. 7, the frequency response of this new-type symmetric bi-planar FSSs at various incident angles for TE and TM polarizations is obtained by utilizing the full-wave simulation software CST. To mimic the infinite new-style structure, floquet ports and unit-cell boundaries are applied in Frequency domain solver.

The frequency response curves of the traditional and the new-type symmetric bi-planar FSSs are depicted in Fig. 8 together. For TE polarization, the curves of new-type symmetric bi-planar FSSs coincide with the traditional one well. While there are some differences existing in the frequency response between the traditional and new type symmetric bi-planar FSSs for TM

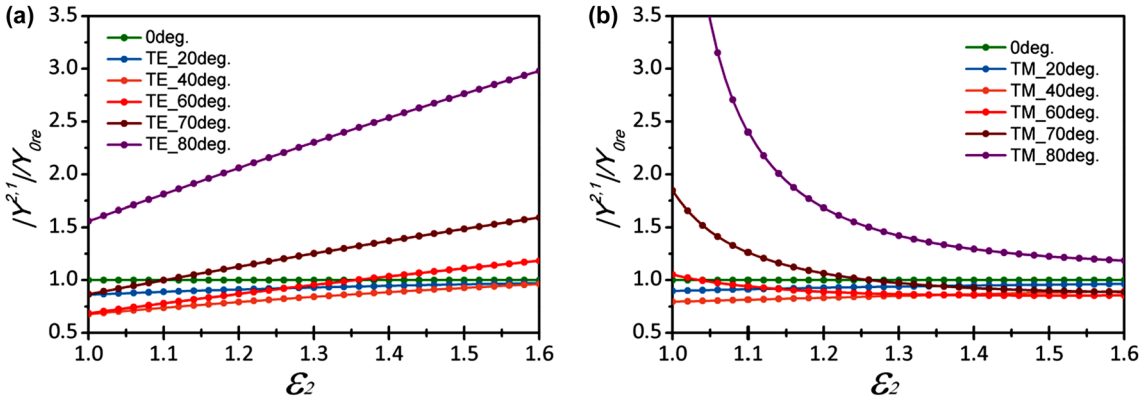

Fig. 4 Ratio $|Y^{2,1}|/Y_{0re}$ with respect to the optimizing ε_2 for **a** TE and **b** TM polarizations at various incident angles from 0° to 80°

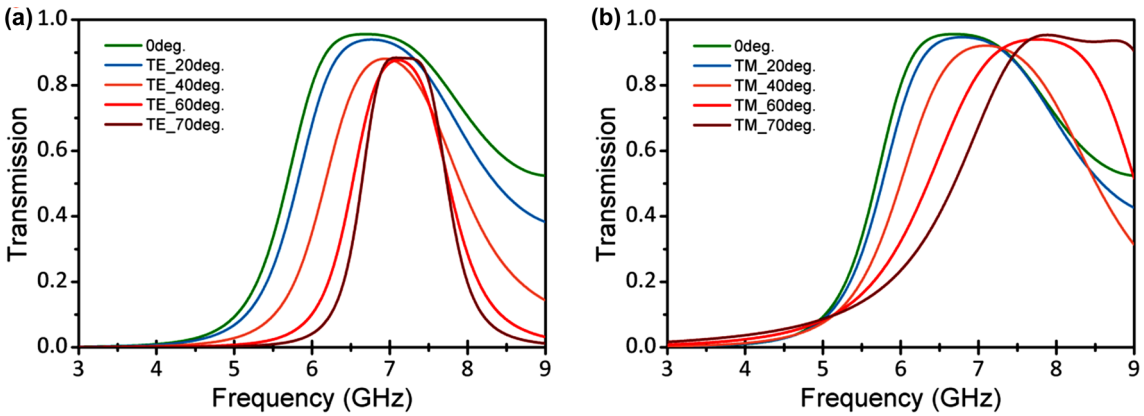

Fig. 5 Frequency response of the symmetric bi-planar FSSs structure with optimizing d_2 and ε_2 (about 15 mm and 1.15) for **a** TE and **b** TM polarizations from 0° to 70°

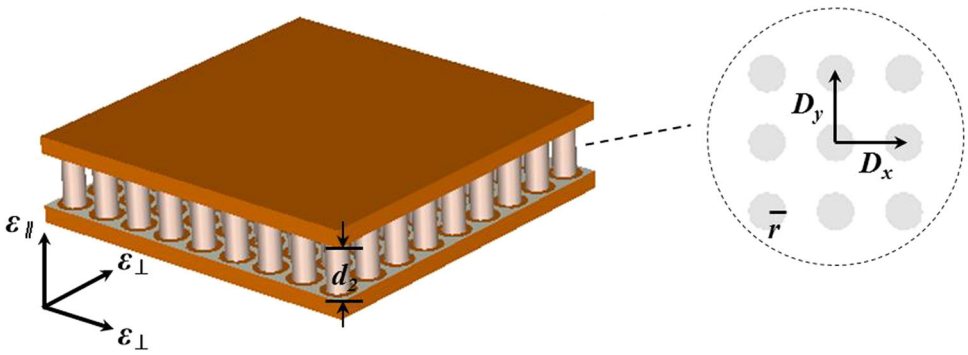

Fig. 6 The new-style symmetric bi-planar FSSs structure

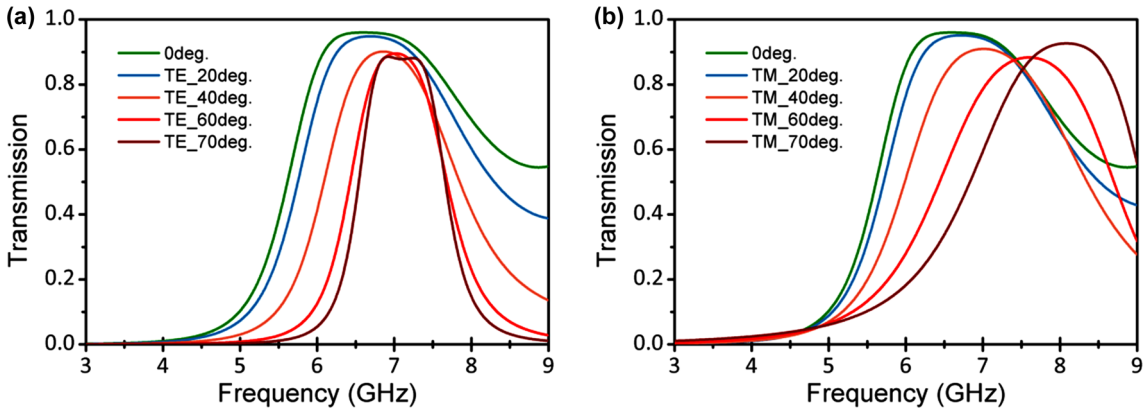

Fig. 7 Transmission curves of the new-style symmetric bi-planar FSSs structure for **a** TE and **b** TM polarizations from normal incidence to 70° incidence

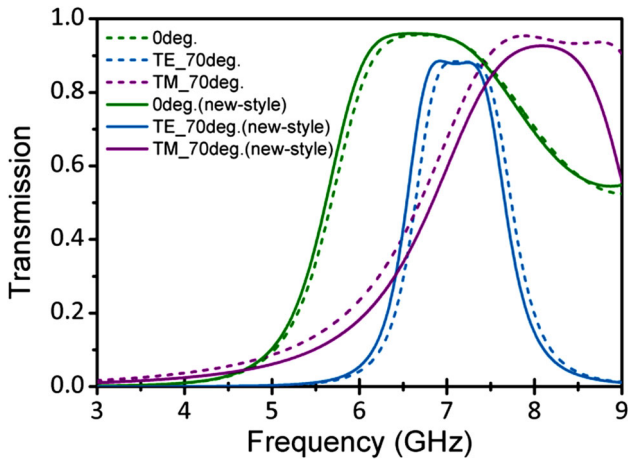

Fig. 8 Comparison of simulation results between traditional and new-style symmetric bi-planar FSSs for various incident angles from 0° to 70°

polarization, which results from the deviation of $\varepsilon_{\parallel}^{eff}(\approx 1.28)$ from 1.15. Although the value of $\varepsilon_{\parallel}^{eff}$ is not equal to 1.15 rigorously, its influence on frequency response can be negligible. These results manifest that an array of dielectric cylinders can effectively replace the homogeneous medium.

4 Fabrication and measurements

To further verify the optimization method and the accuracy of substituting intermediate layer medium with Teflon cylinder arrays, a prototype is fabricated as shown in Fig. 9a. The prototype has a dimension of 420 × 420 mm, and comprises a 30 × 30 array on an axial lattice. It can be fabricated by four steps as follows. First, two identical FSSs backed by 0.0254 mm thin sheets of polyimide are manufactured by using standard printed circuit board photographic and wet-etch techniques. Second, these two FSS screens are, respectively, glued onto two 3 mm quartz-fiber slabs with ethylene-vinyl acetate (EVA) adhesive. The quartz-fiber slab has a permittivity of 3.17 and a tangent loss of 0.008. Then, as depicted in Fig. 9b, dielectric cylinders made of Teflon are carefully glued on top of one FSS screen, simultaneously ensuring that the cylinder and the unit cell of FSS are coaxial. Finally, the other FSS screen is fixed on the top of dielectric cylinders with accuracy alignment.

To verify the accuracy of aforementioned simulation results, the prototype is tested in the free space measurement system depicted in Fig. 9c. This measurement system is composed of an Agilent N5244A vector network analyzer, a pair of lens antennas, a bearing bracket and a

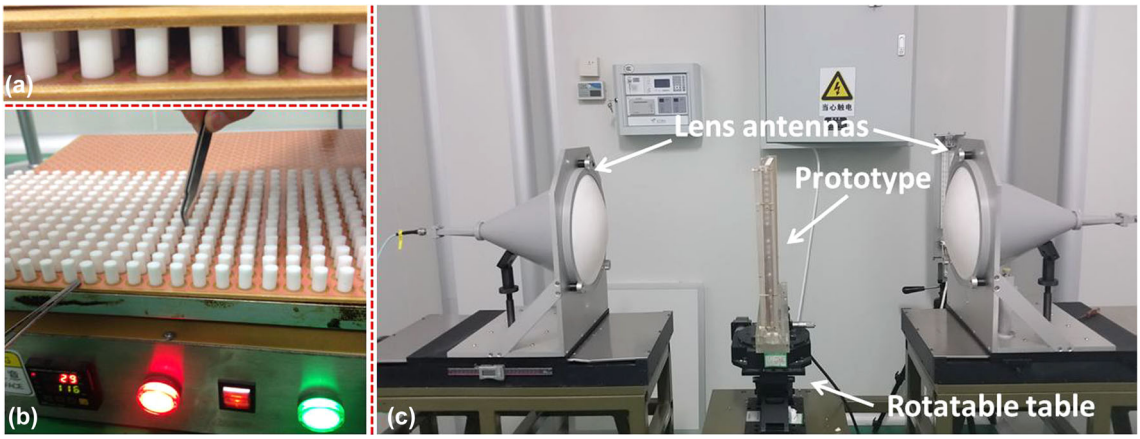

Fig. 9 Photographs of **a** the fabricated prototype, **b** the machining process, and **c** the free space measurement system

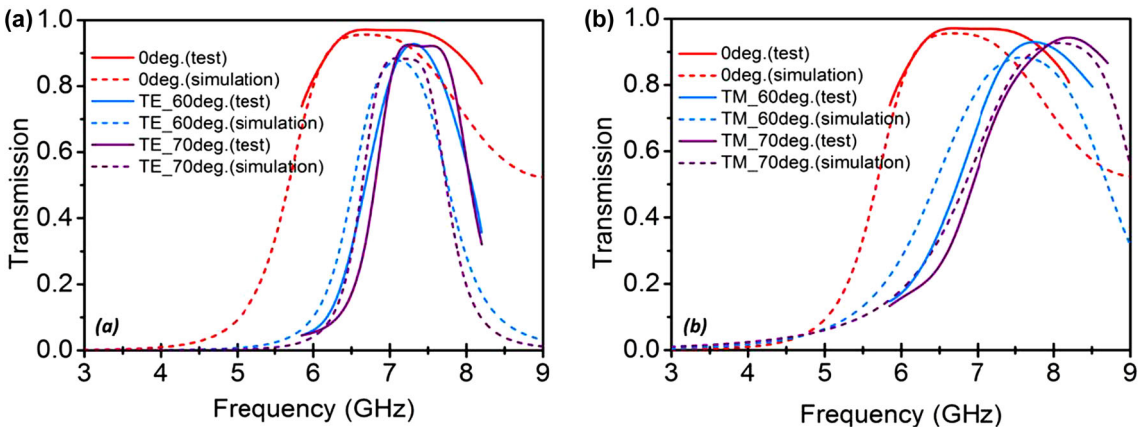

Fig. 10 Contrast of transmission response between simulation and test results for the new-type symmetric bi-planar FSSs structure. **a** TE and **b** TM polarizations

Table 1 Comparison of our prototype with other 3D frequency selective structures

Ref.	Roll-off	1 dB fractional bandwidth (%)	Insertion loss (dB)	Angular stability (°)
This work	1.93	33.98	0.13	0–70
[19]	1.67	13.31	0.15	0–50
[20]	1.39	23.75	0.18	0–40
[21]	1.11	64.13	0.12	0–70
[22]	2.93	18.87	0.8	0–40

rotatable table. The test results are shown in Fig. 10, which surely show the excellent filtering response near 7.4 GHz with flat top (about 400 MHz) and high transmission (more than 80%) from 0° to 70°. To further manifest the filtering curves perform well, the performance of our prototype is compared with those of recent 3D FSS designs [19–22], in term of roll-off, bandwidth, insertion loss and angular stability. The comparison results are listed in Table 1. Note here that, the roll-off is characterized by the ratio of 10 dB bandwidth to 1 dB bandwidth. Therefore, a ratio is closer to one means that the roll-off is steeper. It is seen that our proposed structure can achieve better performance than some of 3D FSS designs. From Fig. 10, we find that the results of measurement and simulation are similar with each other in the same case, except that there is an approximate 200 MHz frequency shift, which may be ascribed to the ignorance of EVA adhesive and polyimide sheets in simulation and fabrication tolerance. The larger test results than simulation results at 60° and 70° angle of incidence are probably caused by the diffraction, as the cross section of prototype decreases with the increment of incident angle. Nevertheless, this experiment positively

verifies the validity of the optimization method and the idea of equivalent substitution.

The physical essence of this proposed FSS structure is a second-order band-pass filter, which is achieved by cascading two identical first-order band-pass filters. Based on the theory of filter, a quarter-wavelength impedance transformer sandwiched between the two first-order band-pass filters is needed, to obtain the ideal Butterworth filtering response. As the optimal coupling medium, the array of dielectric cylinders we adopted plays the same role as the aforementioned impedance transformer in the proposed FSS structure. After a simple calculation, the electrical thickness of coupling layer medium is actually close to quarter-wavelength.

5 Conclusion

In this paper, we propose a simple and fast optimization method for symmetric N layer FSSs structure according to the analysis of self-admittance and mutual admittance. For a symmetric bi-planar FSSs structure with specified top and bottom layers medium, the optimum parameters of intermediate layer (thickness and permittivity) can be obtained easily by utilizing this method. The full wave simulation results of the optimized structure show a quite good filtering effect with broad flat top and sharp roll-off at 70° incidence, which proves the correctness of the optimizing method. As the optimum permittivity of 1.15 is difficult to obtain using traditional technique, an array of dielectric cylinders made of Teflon is designed to substitute the intermediate layer medium, based on the theory of periodic waveguides. The approximate permittivity of the Teflon cylinders array can be modulated by the fill factor of dielectric cylinder. An excellent match between simulation and test results further validates the idea of designing materials that non-existent in nature.

Acknowledgements This work is supported by the National Natural Science Foundation of China (Grant No. 61172012).

References

1. M.Z. Joozdani, M.K. Amirhosseini, A. Abdolali, Electron. Lett. **52**, 767–768 (2016)
2. Y.C. Hou, W.J. Liao, C.C. Tsai, S.H. Chen, I.E.E.E. Trans, Antennas Propag. **64**, 1859–1867 (2016)
3. L.Y. Li, J.F. Wang, H. Ma, J. Wang, M.D. Feng, H.L. Du, M.B. Yan, J.Q. Zhang, S.B. Qu, Z. Xu, Appl. Phys. Lett. **108**, 122902 (2016)
4. S.M. Mahmood, T.A. Denidni, I.E.E.E. Antenn, Wirel. Pr. **15**, 1148–1151 (2016)
5. M.N. Jazi, M.R. Chaharmir, J. Shaker, A.R. Sebak, I.E.E.E. Trans, Antennas Propag. **64**, 99–108 (2016)
6. C. Saeidi, D.V. Weide, Appl. Phys. Lett. **103**, 183101 (2013)
7. S. Sui, H. Ma, J.F. Wang, Y.Q. Pang, S.B. Qu, J. Phy. D: Appl. Phys. **48**, 215101 (2015)
8. J.Y. Yin, X. Wan, Q. Zhang, T.J. Cui, Sci. Rep. **5**, 12476 (2015)
9. J.D.B. Filgueira, A.L.P.S. Campos, A.G. Neto, R.H.C. Manicoba, Micro. Optical Technol. Lett. **58**, 1984–1989 (2016)
10. Y. Zhao, M.A. Belkin, A. Alù, Nat. Comm. **3**, 870 (2012)
11. C. Pfeiffer, C. Zhang, V. Ray, L.J. Guo, A. Grbic, Phys. Rev. Lett. **113**, 023902 (2014)
12. C. Menzel, J. Sperrhake, T. Pertsch, Phys. Rev. A **93**, 063832 (2016)
13. Z. Yang, Z.H. Xue, W.M. Li, X. Lv and W. Ren, IEEE ISAPE, 755–758 (2008)
14. C. Mateo-Segura, G. Goussetis, A.P. Feresidis, I.E.E.E. Trans, Antennas Propag. **58**, 2523–2530 (2010)
15. P.S. Taylor, E.A. Parker, J.C. Batchelor, I.E.E.E. Trans, Antennas Propag. **59**, 3265–3271 (2011)
16. B.A. Munk, *Frequency-selective surfaces: theory and design* (Wiley, New York, 2000)
17. M. Kuittinen, J. Turunen, P. Vahimaa, *Subwavelength-structured elements in diffractive optics for industrial and commercial applications* (Cambridge University Press, New York, 1998)
18. A. Lehmuskero, B.F. Bai, P. Vahimaa, M. Kuittinen, Opt. Express **17**, 5481–5489 (2009)
19. K. Tao, B. Li, Y. Tang, M. Zhang, Y. Bo, Electron. Lett. **53**, 324–326 (2017)
20. S. Can, E. Karakaya, F. Bagci, A.E. Yilmaz, B. Akaoglu, ETRI J. **39**, 69–75 (2017)
21. C. Pelletti, R. Mittra, G. Bianconi, IEEE ISAPD, 1–2 (2012)
22. B. Li, Z. Shen, IEEE Trans. Microw. Theory Tech. **61**, 3578–3589 (2013)